JOURNAL OF PROPULSION AND POWER
Vol. 16, No. 1, January–February 2000

Computational Analysis of Stall and Separation Control in Centrifugal Compressors

Alex Stein,* Saeid Niazi,* and L. N. Sankar†
Georgia Institute of Technology, Atlanta, Georgia 30332

A three-dimensional compressible Navier–Stokes code has been used to model the steady and unsteady flowfield within a low-speed centrifugal compressor configuration tested at NASA Lewis Research Center. Near-design conditions, the performance map, pressure field, and the velocity field were in good agreement with measured data. At off-design conditions, the calculations show that flow reversal first occurs near the blade leading edge. If left unchecked, the reversed-flow region grows spatially and temporally. Injection of air upstream of the compressor face was found to modify the local flow near the blade leading edge and to suppress rotating stall and surge. Even a moderate amount of air, typically around 5% of the total mass flow rate, was sufficient to extend the useful operating range of the compressor.

Nomenclature

A	= area
$\boldsymbol{F}$	= inviscid flux vector
$\dot{m}$	= mass flow rate
$\boldsymbol{n}$	= unit normal vector
P_0	= stagnation pressure
p	= static pressure
$\boldsymbol{q}$	= state vector
$\boldsymbol{R}$	= viscous flux vector
R_{Inlet}	= leading-edge tip radius
S	= surface
t	= time
t^*	= time at instance of part-span stall
U_t	= leading-edge tip velocity
$\boldsymbol{V}$	= velocity vector
$\boldsymbol{V}_G$	= vector of grid velocities
α, β	= injection angles
ρ	= density

Subscripts

in	= inflow property
n	= normal property
out	= outflow property
∞	= far-field property

Introduction

CENTRIFUGAL compressors are currently being used in turbine engines' powering tanks and rotorcraft. This is mainly due to their ability to produce high-pressure ratios with fewer stages than axial compressors, leading to an overall reduction in size and weight. However, the useful operating range of a centrifugal compressor is limited by the unsteady flow phenomena that occur at low mass flow rates. These aerodynamic phenomena are rotating stall and surge.

Rotating stall is a local phenomenon in which a circumferentially uniform flow pattern is disturbed, and some of the blades experience stall. The stalled regions move from blade-to-blade, and appear to rotate about the shaft axis, at an angular velocity that is one-third to one-half that of the shaft angular velocity. Rotating stall may lead to vibrations and fatigue of the compressor blades, and is often a precursor to surge. It is to be avoided at all costs.

Surge is a global one-dimensional instability that can affect the whole compression system. It is accompanied by low-frequency fluctuations in pressure and mass flow rate. If surge is severe enough, even complete flow reversal is possible.

To avoid these instabilities, the designer is forced to introduce a safety margin of typically 20% between the stall (or surge) line and the engine operating condition, thus decreasing the efficiency of the compressor. In the past, many attempts have been made to reduce this margin by using appropriate stall detection and control devices. Over the last five decades, a number of experimental studies have been conducted for axial compression systems.[1–6] Centrifugal compressor stall and surge control have not been studied in nearly as much detail because of the geometric complexity of centrifugal impellers, and due to the difficulties in visualizing the flow and measuring velocity and pressure fields within blade passages. References 7–11 are representative examples of experimental studies aimed at controlling centrifugal compressor stall and surge.

Computational fluid dynamics (CFD) methods provide an efficient way to study these complex flow phenomena. Because of the massive increase in computing power and the development of sophisticated flow-visualization tools, it is now possible to do three-dimensional real-time simulations of compression systems. Engine industries routinely use CFD methods for compressor and turbine system design. Many of these methods are also suitable for modeling stall and surge, and are convenient vehicles for testing novel control strategies.

A number of CFD codes for detailed modeling of turbomachinery flowfields exist. Chima and Yokota,[12] Hall,[13] Dawes,[14] Hah and Wennerstrom,[15] and Adamczyk et al.,[16] among others, have developed three-dimensional codes that are capable of analyzing unsteady turbomachinery flow with multiple blade passages and/or rotor–stator interaction. Most of these applications, however, have been limited to modeling the steady-state phenomena in axial and centrifugal compressors, or for modeling unsteady flow phenomena caused by rotor–stator interactions. Many researchers have also simulated rotating stall and surge in axial compressors using simple one- and two-dimensional codes.[17,18] Three-dimensional simulations of stall and surge have not been done due to the computational resources required.

In an effort to model unsteady flow within centrifugal compressors, the present authors have developed a three-dimensional unsteady flow solver. Preliminary code validation studies for a NASA Lewis Research Center low-speed centrifugal compressor (LSCC) configuration were reported in Ref. 19. In Ref. 19, this CFD code

Presented as Paper 98-0934 at the AIAA 36th Aerospace Sciences Meeting, Reno, NV, 12–15 January 1998; received 11 August 1998; revision received 15 January 1999; accepted for publication 16 January 1999.

*Graduate Research Assistant, School of Aerospace Engineering. Student Member AIAA.

†Regents' Professor, School of Aerospace Engineering. Associate Fellow AIAA.

was also used to study the effect of steady bleeding on the performance of the compressor. It was shown that bleed valves placed in the diffuser walls help to improve the flow pattern within the diffuser, and eliminate diffuser stall. However, bleeding has the disadvantage of removing useful, high-pressure air from the system, thereby decreasing the overall efficiency of the system. Murray[20] also showed that a compression system that utilizes a bleed valve controller is ultimately not stabilizable, it can only achieve operability enhancements.

As mentioned earlier, various alternatives to bleeding have experimentally been tested. Such control strategies include movable plenum walls, inlet guide vanes, and air-injection jets upstream of the compressor face. In these approaches, the presence of a growing instability (stall precursor waves) is first detected. A countering fluid–mechanical disturbance is introduced in the flowfield, effectively canceling and eliminating the instability. Because rotating stall is detected and eliminated before it grows into a fully developed surge, a relatively small amount of control power may be sufficient. There is a need for systematic computational models of these control devices to help understand how and why they work.

The present study is aimed at modeling and understanding the effects of air injection on the operation of the compressor. Steady and unsteady flow results in the form of performance map, velocity fields, and pressure data are presented for the NASA LSCC configuration. Details of the flowfield are discussed that explain how air injection enhances the performance of the centrifugal compression system.

It should be noted that the current study is limited to the simulation of a single blade passage, thus taking advantage of the blade-to-blade periodicity in centrifugal compressors. This approach was chosen to reduce the overall grid size and to keep computational expenses at a reasonable level. However, as a result of this, instabilities that propagate in the circumferential direction and are of greater-than-blade-width length scales (rotating stall) cannot be modeled within the scope of this study. Instead, this research and the applied control methodology (air injection) focus on the development, understanding, and avoidance of global one-dimensional instabilities (surge).

Numerical Formulation

The mathematical and numerical formulation behind the three-dimensional flow solver used in this study has been described in Ref. 19. Therefore, only a brief description of the formulation is given here.

The three-dimensional unsteady compressible Reynolds-averaged Navier–Stokes equations are solved in strong conservation form. This involves solving the governing equations using a control volume form. An implicit time-marching procedure is used, starting from an initial flow condition, with appropriate boundary conditions. The governing equations in integral form can be written as

$$\frac{\partial}{\partial t}\iiint_V q\,\mathrm{d}V + \oiint_S (\boldsymbol{F} - q\boldsymbol{V}_G)\cdot\boldsymbol{n}\,\mathrm{d}S = \oiint_S (\boldsymbol{R})\cdot\boldsymbol{n}\,\mathrm{d}S \quad (1)$$

Here, V and S refer to the control volume and control surfaces, respectively. The viscous fluxes $\boldsymbol{R}$ are computed explicitly, whereas the inviscid fluxes $\boldsymbol{F}$ are calculated implicitly using Roe's approximate Riemann solver.[21] $\boldsymbol{V}_G$ is the grid velocity in an inertial coordinate system to account for the rotor motion. To solve the system of equations, first, a three-factor alternating direction implicit scheme[22] is used to factorize the implicit coefficient matrix operator into block tridiagonal matrices. Then, the equations are solved using the Thomas algorithm.[23] This makes the scheme first-order accurate in time. To model the effect of turbulence, the one-equation Spalart–Allmaras[24] model is used.

Flow through only a single blade passage has been studied in the present approach. Simple blade-to-blade periodic conditions are implemented in the code. No-slip boundary conditions are used at all solid walls. At these surfaces, density and pressure are extrapolated from the interior. In the inlet, the stagnation pressure, stagnation temperature, and flow angles are prescribed. The static pressure at the exit is prescribed. A one-dimensional Riemann characteristic wave equation is solved at the inlet, allowing the acoustic disturbances to leave the computational field through the inlet face. At the exit, entropy and vorticity are also extrapolated from the interior.

Results and Discussion

The geometry chosen to simulate compressor stall control is the NASA LSCC configuration, shown in Fig. 1. This impeller has extensively been tested by Hathaway et al.[25] and Wood et al.[26] at the NASA Lewis Research Center, providing a well-documented case for CFD code validation purposes. The compressor characteristics are given next: Impeller: 20 full blades with 55-deg backsweep; inlet diameter: 0.87 m; exit diameter: 1.52 m; tip clearance: 2.54 mm (1.8% of blade height at trailing edge); and design conditions: mass flow rate = 30 kg/s, rotational speed = 1862 rpm, total pressure ratio = 1.14, and adiabatic efficiency = 0.922. Several researchers[26–29] have performed CFD studies of this compressor and compared their results with measured data at compressor design conditions. They generally observed good agreement between the computed and experimental results. Areas of relatively poor agreement, the impeller blade loading and flow details in or near the tip clearance gap, were identified and addressed in some detail.

The computational grid used to model the single compressor flow passage is shown in Figs. 1 and 2. It has dimensions of $129 \times 61 \times 41$ in the streamwise, spanwise, and pitchwise directions, respectively. Four cells are used in the clearance gap between the blade tip and the compressor casing. Most calculations with this mesh were carried out on a Silicon Graphics Origin 2000 with four processors, though using only a single processor per run. The code executes at about 2×10^{-5} s per point per time running in a time-accurate mode. Although the present implicit scheme can use large time

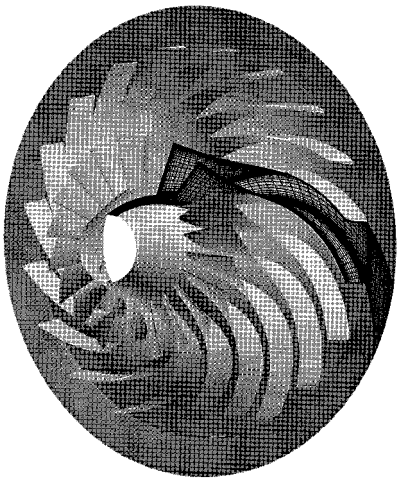

Fig. 1 Perspective view of single flow passage grid for NASA LSCC.

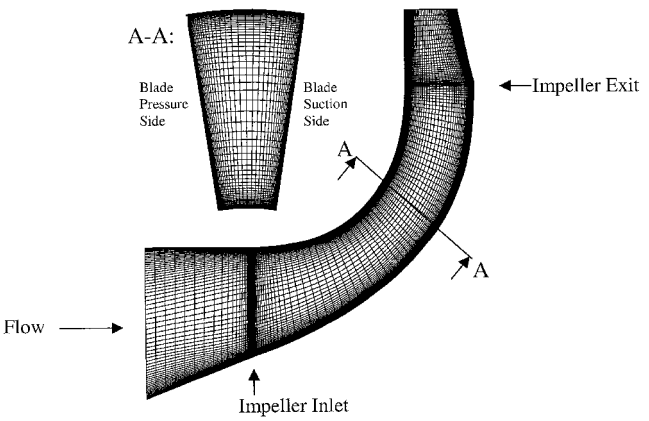

Fig. 2 Grids in streamwise and meridional plane.

steps, the Courant–Friedrichs–Lewy number was kept at or below 2 for resolving the unsteady flow in a time-accurate manner. The calculations were generally run for $1\frac{1}{2}$–2 compressor revolutions, before a steady state or a limit-cycle oscillation (indicative of separation and/or surge) was achieved. The mass flow rate across several streamwise planes was monitored and used as a convergence criterion.

A limited number of grid sensitivity studies were done to ensure the spatial accuracy of the flow solver. For this purpose, the compressor performance map was calculated with the baseline grid described earlier, and with a coarse grid that consists of every other grid point of the baseline mesh. To construct the performance map, the compressor code was run with various exit pressures to give the desired mass flow rate for the particular setting. This corresponds to a real compressor where the mass flow rate is controlled by a plenum throttle valve. The total pressure rise across the impeller was found by mass averaging the stagnation pressure across each streamwise plane. The pressure ratio then becomes

$$\Delta p_0 = \frac{p_{0,\text{out}}}{p_{0,\text{in}}} = \frac{(\iint_A p_0 \rho u \, \mathrm{d}A / \iint_A \rho u \, \mathrm{d}A)\big|_{\text{out}}}{(\iint_A p_0 \rho u \, \mathrm{d}A / \iint_A \rho u \, \mathrm{d}A)\big|_{\text{in}}} \tag{2}$$

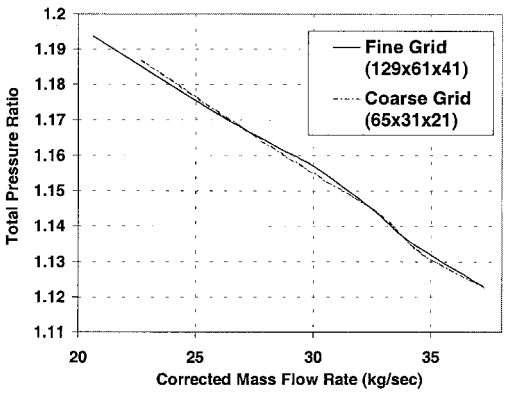

Fig. 3 Comparison between performance map using fine grid and coarse grid.

The comparison between the fine and the coarse grid performance map shown in Fig. 3 revealed no great discrepancies. Initially, it seemed that the flow simulations obtained with the coarse mesh yielded satisfactory results. However, a more detailed study of the flowfield, particularly the region in and near the clearance gap, showed that the baseline fine grid should be used to obtain a better resolution of certain flow features. Thus, all subsequent results in this paper are based on this baseline (fine) mesh.

Results at Design Conditions

Figure 4 shows a comparison between computed and measured blade pressure contours. Results are shown near the blade pressure surface and the blade suction surface. Good agreement between the computed and measured data is observed in most flowfield regions. Both the CFD and the experimental data show a region of minimum pressure near the leading-edge blade tip of the suction side. As the fluid enters the impeller region, it first experiences a sudden acceleration, similar to the case of an airfoil at an angle of attack. This increase in velocity is accompanied by a decrease in static pressure. On both blade surfaces throughout the impeller the highest pressure occurs on the hub, and decreases gradually along the span of the blades. This is because the pressure in this plot is shown without its centrifugal contribution. In general, the pressure rise across a centrifugal compressor stage consists of 1) the pressure rise due to the work done on the fluid by the compressor, and 2) the increased turning of the fluid away from the rotation axis resulting in an acceleration of the flow:

$$p_{\text{static}} = p_{\text{compr}} + p_{\text{centr}} = p_{\text{compr}} + \tfrac{1}{2}\rho V^2 \tag{3}$$

To emphasize the pressure rise due to work done on the fluid, the static pressure rise in Fig. 4 is shown without its centrifugal part p_{centr}.

A region that shows discrepancies between the CFD and the experimental data is located near the shroud on the pressure surface (~140% chord length). Here, the CFD data show a region of high gradients that is not reflected in the experimental data. It is unclear whether this phenomena is due to insufficient CFD modeling or to a loss in information due to the spatial averaging applied experimentally.

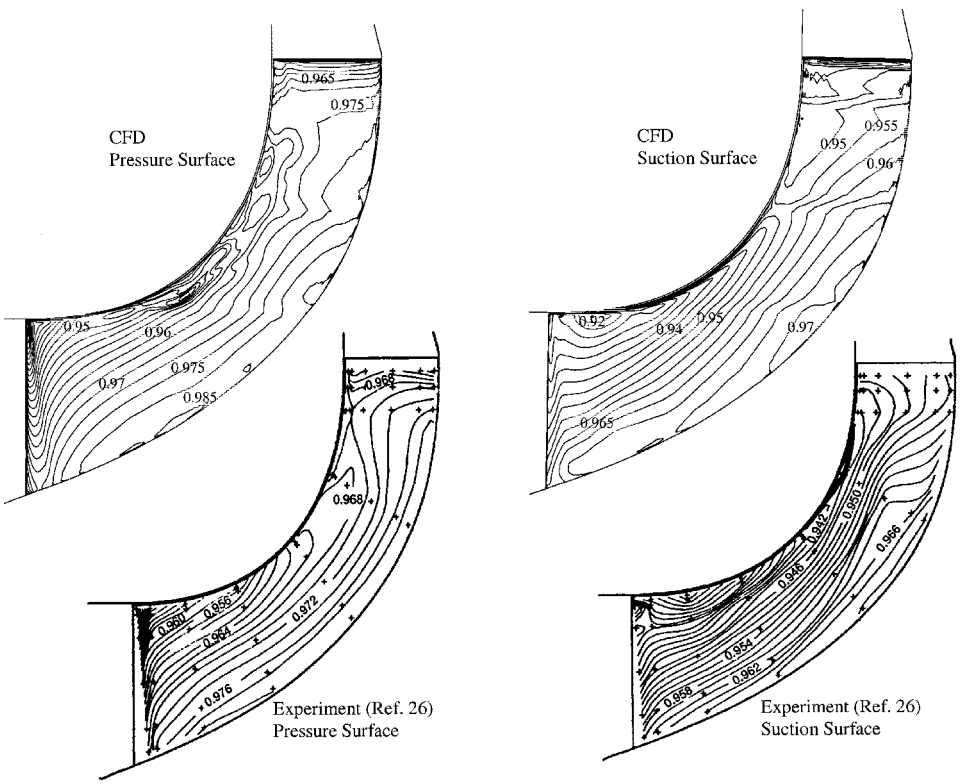

Fig. 4 Comparison between computed and measured[25] surface pressure p/p_∞ at design conditions.

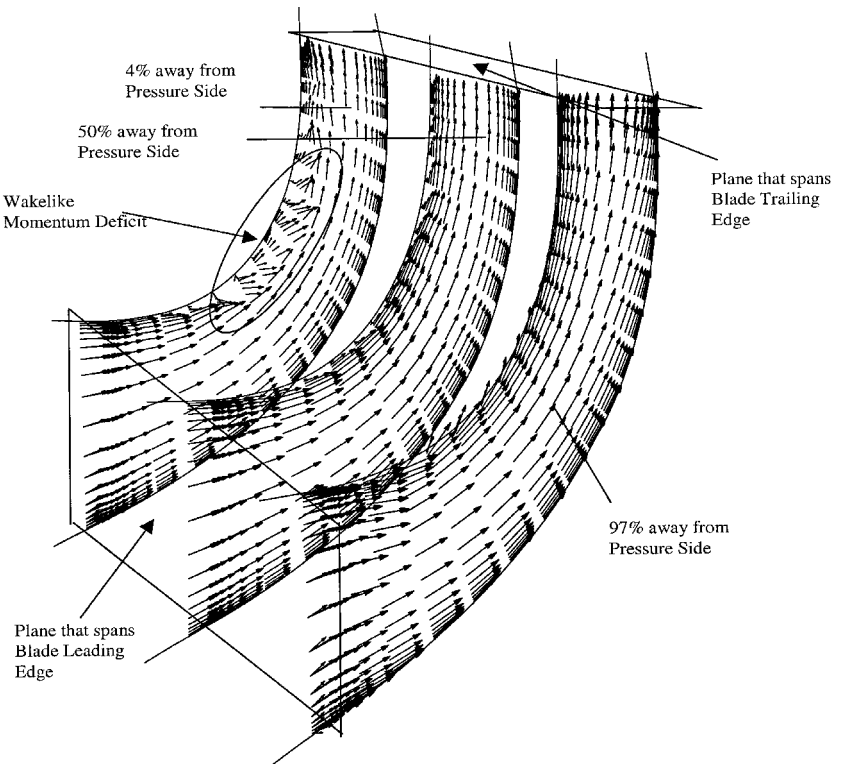

Fig. 5 Velocity field in meridional planes 4, 50, and 97% away from the blade pressure surface at design conditions.

Figure 5 shows the development of the impeller throughflow in the form of vector plots. In these plots the velocity vectors were obtained by transforming the three-dimensional velocity field into the x–r-meridional plane. Three such planes with projected velocity vectors are shown: 4, 50, and 97% away from the blade pressure surface. In each plane the overall flowfield is well behaved and attached. Small regions of reversed flow are present near the compressor shroud. This separation zone is part of a throughflow momentum deficit that exists in the outer 10–20% of the span. The same wakelike phenomenon was reported by Hathaway et al.,[29] who experimentally analyzed the NASA LSCC configuration. They concluded that this momentum deficit is generated as a result of the tip clearance flow. This phenomenon has also been observed in several centrifugal compressor facilities by other researchers. It will be shown in this paper that this wake will eventually develop into a strong reversed-flow region and lead to a stalled condition when the mass flow rate through the compressor is reduced.

To address this issue, the compressor flowfield was calculated for different operating conditions, parametrically changing the back pressure. Figure 6 shows the comparison between the calculated and the experimental performance map on the right, stable branch of the curve. Both data show the same quantitative behavior. However, the CFD results overestimate the pressure rise by about 1.5%. The authors believe that this slight discrepancy is due to an insufficient modeling of some flow details that would contribute to a reduction in total pressure; e.g., tip clearance, turbulence modeling. For operating conditions below 20 kg/s, strong limit-cycle oscillations in several flow properties (mass flow rate, pressure) were observed. This is in agreement with the experimental report by Hathaway et al.,[25] who reported audible unsteady flow conditions for operating points just below 20 kg/s.

The time history for four selected points, A–D of the performance map, is shown in Fig. 7. The four points were chosen as A: mass flow rate = 32.5 kg/s (stable operation); B: mass flow rate = 20.5 kg/s (onset of stall); C: uncontrolled, stalled operation; and D: mass flow rate = 17.5 kg/s, injected mass flow rate = 1.75 kg/s (controlled operation, 10% air injection).

Plots A–D in Fig. 7 show the amount of fluctuations (in %) in mass flow rate and pressure rise at each operating condition, respectively.

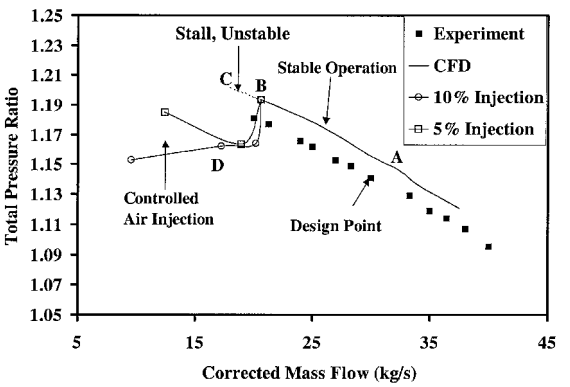

Fig. 6 NASA LSCC performance map; comparison between computed and measured[25] data.

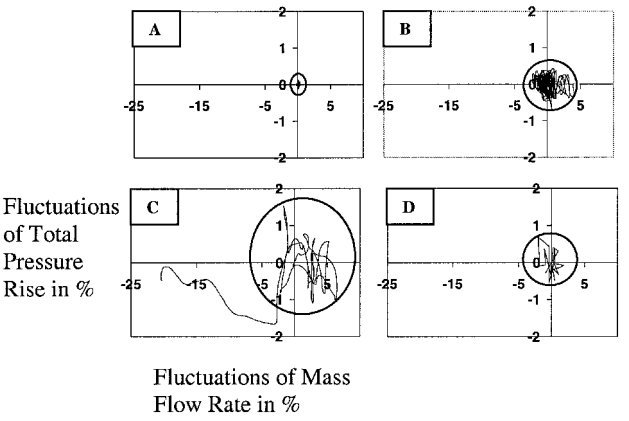

Fig. 7 Total pressure rise fluctuations (in %) vs mass flow rate fluctuations (in %) for selected points A–D.

These plots are similar to the Poincaré maps used to study chaos in nonlinear systems. At the stable operating point (referred to as an attractor) A, fluctuations in mass flow rate and pressure rise are limited to just 0.2–0.3%. As the mass flow rate is decreased, the fluctuations grow to 3–4% near the onset of stall (point B), but remain bounded about the attractor. A further reduction in mass flow rate causes the oscillations to grow unbounded with time, which eventually drives the system to a stalled condition. In this case, much of the flow through the impeller is reversed, and the compressor is surging. In addition to Fig. 7, the time history of the mass flow rate fluctuations (in %) for points A, B, and C is shown in Fig. 8. This plot underlines the growth of instabilities at a reduced mass flow rate. It is interesting to note that at the onset of stall (point B), the frequency of mass flow rate and the rotational frequency are of the same order (30 Hz).

To improve the characteristic map, the flowfield at the onset of stall was studied in detail, and results in vector plots at the midpassage meridional plane for different time steps are shown in Fig. 9. Figure 9 shows that the local reverse flow originates in the leading-edge region of the impeller blades. This reversed-flow region grows rapidly in size and extends to the diffuser, leading to large mass flow rate fluctuations and stall after three cycles.

Results at Off-Design Conditions and Stall Control

Considerable experimental evidence exists that air injection in a steady or unsteady fashion improves the overall operability of the compressor. By properly designing fast-acting injection valves and placing them upstream of the compressor face, various researchers were able to achieve operation stability and a significant increase in stall margin. However, to date, a certain degree of confusion exists in the compressor community as to why air injection is successful. Day[30] proposed that the suppression of stalling disturbances and the removal of stalling cells be the primary mechanism. Weigl et al.[31] attributed the increase in operability to the additional momentum added by the jets that increases the total pressure at the rotor inlet and

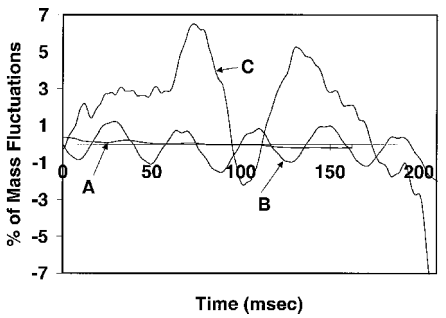

Fig. 8 Mass flow rate fluctuations (in %) vs time (in ms) for selected points A–C.

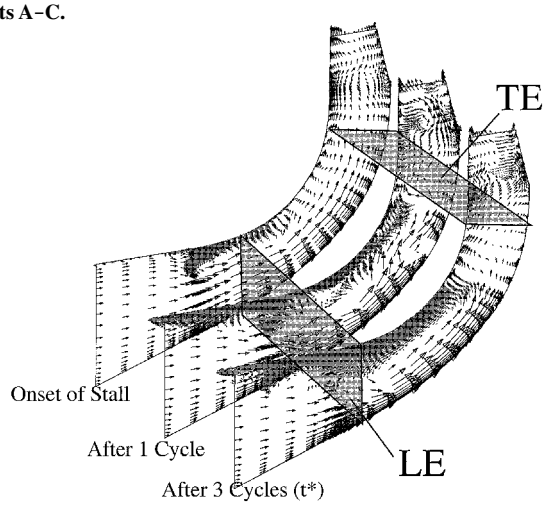

Fig. 9 Velocity field near midpassage at onset of stall, after 1 and 3 revolutions.

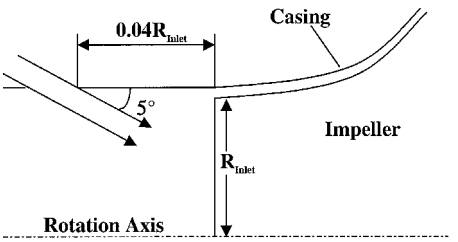

Fig. 10 Schematic of injection characteristics for NASA LSCC.

suppresses separated and/or reversed flow. Together with Murray,[20] Weigl et al.[31] unanimously concluded that air injection inherently modulates the shape of the performance map and shifts the last stable operating point to lower mass flow rates.

In this study, uniform, steady air injection was used. Such types of injection may not be efficient for use in a practical compressor system because of the high-pressure air supply needed to operate the injection system. It may be better to incorporate the injection actuators in a closed loop with appropriate stall sensors and a controller unit to activate the injectors only if the compression system experiences any onset of stall. Air injectors can be configured in many ways; typically a number of injection valves are located upstream of the compressor face on the circumference of the compressor casing. The proper choice of injector characteristics (injected mass flow rate, injection angle, yaw angle) may vary from system to system. Figure 10 shows a schematic of the simulated annular flush slot injectors used in this study. The injection geometry was configured to inject an axisymmetrical sheet of high-momentum air along the casing wall into the rotor tip region. The injection angle α was 5 deg, the yaw angle β was zero (injection perpendicular to compressor face), and the injected mass flow rate was either 5 or 10% of the throughflow mass flow rate. The amounts of injected air were chosen based on previous experimental studies by Weigl et al.[31] and Giffin and Smith,[32] who applied injection control to compressors using 1.5–5.8% and 4% injected mass flow rates, respectively. In this spirit, a 5% blowing fraction can be categorized as a reasonable choice, a 10% blowing fraction would be a high value to be applied in an industrial compressor. However, for the purpose of investigating the physical processes, the numbers can be considered reasonable. To implement the air-injection scheme into the CFD flow solver, the velocity along the injector boundaries was prescribed to yield the desired injection rates and angles. The remaining flow properties, density and pressure, were extrapolated from the interior. The compressor mass flow rate in the case of air injection was then determined at the compressor exit.

Figures 11a and 11b show photographs of regions near the impeller leading edge that experience reversed flow (regions with negative streamwise velocity). The figure compares flowfield simulations with and without air injection. It is evident in the case without injection that much of the impeller flow passage sees reversed flow (part-span stall or mild surge), which will eventually lead to the complete stall of the compressor (full-span stall or deep surge). This instantaneous operating condition shown in Figs. 11a and 11b corresponds to point C on the performance map discussed earlier in Fig. 6. The transient response of the compressor when operated with this throttle setting is plotted in Fig. 7 (plot C). The compressor undergoes large fluctuations in mass flow rate (5–10%) until a complete stall condition is encountered.

Figure 11b demonstrates that by injecting 10% of the mass flow rate into the main flow, much of the stalled reverse-flow regions disappear, and the compressor is able to operate at a stable operating condition. Referring back to the performance map [Fig. 7 (plot D)] shows the transient response of the compressor when operated with 10% air injection (at mass flow rates below point B only). Fluctuations of mass flow rate and pressure are very small (2–3%). The useful operating range of the compressor for 5 and 10% air injection has been extended to 12.5 and 10 kg/s, respectively, ~60% below the design condition of 30 kg/s.

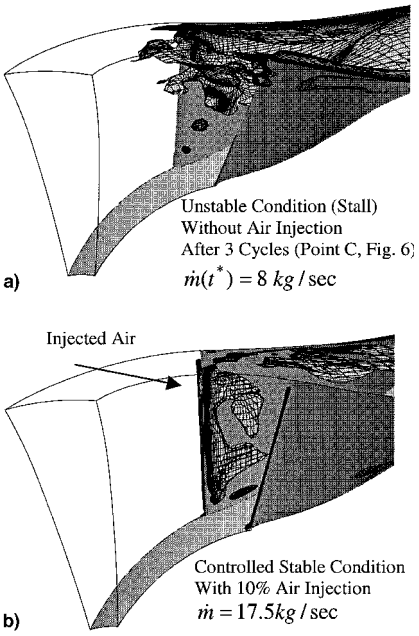

Fig. 11 Regions with negative streamwise velocity.

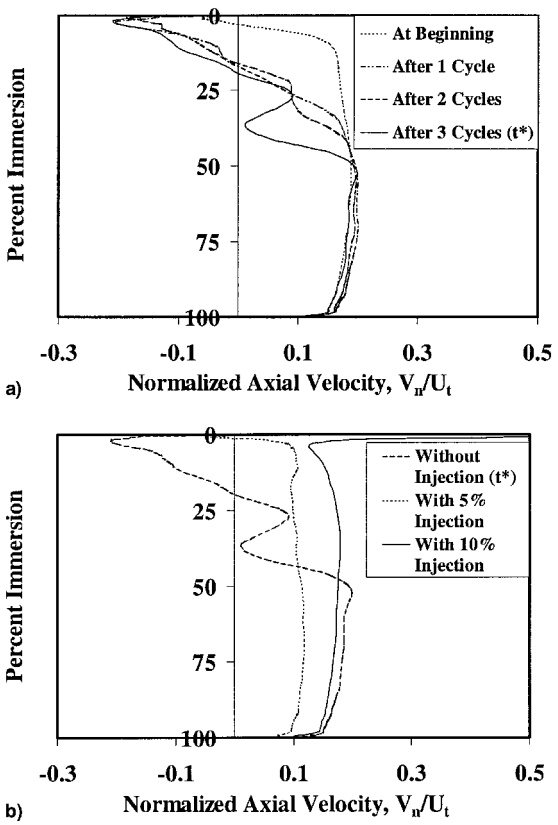

Fig. 12 Circumferentially averaged spanwise distribution of axial velocity: a) without injection for different cycles and b) comparison between injection and no injection.

In an attempt to understand why and how the air-injection mechanism works, the flowfield was examined after various impeller revolutions (cycles). Figures 12a and 12b show a comparison between normalized axial velocities at points C (stalled, unstable condition after different number of cycles) and D (stable condition, with air injection). The data were taken at a distance $0.11R_{Inlet}$ upstream of the compressor face and were referenced by the impeller exit tip speed $U_t = 153$ m/s. It is seen that local reversed-flow regions first originate near the blade leading edge. This may be due to the separation at the blade leading edge, which has a small leading-edge radius. Associated with this local unsteady separation are the local pressure fluctuations, or the so-called precursor waves. Precursor waves are small short-length fluctuations in flow properties (density, pressure, etc.) that are indicative of the beginning development of compressor instabilities such as rotating stall. If no attempt is made to eliminate this leading-edge separation, the reversed-flow region grows in size and envelops much of the inlet (shown in Fig. 11a). When air is injected into the main flow at an appropriate angle, even in small quantities, the local effective angle of attack is decreased, and the flow in the leading-edge region reattaches; the reversed-flow regions near the leading edge disappear (shown in Fig. 11b), and the compressor returns to a stable operating regime.

Conclusions

A computer code for modeling single and multistage centrifugal compressors has been developed and validated. At reduced mass flow off-design conditions, local reversed flow was first found to occur in the leading-edge region of the impeller blades. If left unchecked, this reversed-flow region grew rapidly in size, leading to an uncontrolled growth in the mass flow rate and pressure rise fluctuations. Injection of air at the compressor face was seen to eliminate the local separation and extend the useful operating range of the compressor. Even a moderate amount ($\sim 5\%$) of injected mass was sufficient to eliminate the leading-edge flow reversal and return to a controlled, stable operation.

Acknowledgments

The authors were supported by the U.S. Army Research Office under the Multidisciplinary University Research Initiative on Intelligent Turbine Engines. David Mann was the Technical Monitor. The authors are thankful to Michael Hathaway of the U.S. Army Vehicle Technology Center for supplying the grid, experimental pressure, and performance data, and for numerous suggestions during the course of this study.

References

[1] Iura, T., and Rannie, W. D., "Experimental Investigations of Propagating Stall in Axial Compressors," *ASME Transactions*, Vol. 76, No. 3, 1954, pp. 463–471.

[2] Emmons, H. W., Pearson, C. E., and Grant, H. P., "Compressor Surge and Stall Propagation," *ASME Transactions*, Vol. 77, No. 1, 1955, pp. 455–469.

[3] Greitzer, E. M., "Surge and Rotating Stall in Axial Compressors, Parts I and II," *Journal of Engineering for Power*, Vol. 98, No. 2, 1976, pp. 190–216.

[4] Moore, F. K., "A Theory of Rotating Stall of Multistage Axial Compressors," *Journal of Engineering for Gas Turbine and Power*, Vol. 106, No. 2, 1984, pp. 313–336.

[5] Longley, J. P., "A Review of Nonsteady Flow Models for Compressor Stability," *Journal of Turbomachinery*, Vol. 116, No. 2, 1994, pp. 202–215.

[6] Paduano, J. D., "Active Control of Rotating Stall in Axial Compressors," Ph.D. Dissertation, Dept. of Aeronautics and Astronautics, Massachusetts Inst. of Technology, Cambridge, MA, 1991.

[7] Gysling, D. L., Dugundji, J., Epstein, A. H., and Greitzer, E. M., "Dynamic Control of Centrifugal Compressors Using Tailored Structures," American Society of Mechanical Engineers, Paper 90-GT-122, 1990.

[8] Pinsley, J. E., Guenette, G. R., Epstein, A. H., and Greitzer, E. M., "Active Stabilization of Centrifugal Compressor Surge," American Society of Mechanical Engineers, Paper 90-GT-123, 1990.

[9] Lawless, P., and Fleeter, S., "Active Unsteady Aerodynamic Suppression of Rotating Stall in an Incompressible Flow Centrifugal Compressor with Vane Diffusers," AIAA Paper 91-1898, June 1991.

[10] Toyama, K., Runstadler, P. W., and Dean, R. C., "An Experimental Study of Surge in Centrifugal Compressors," *Journal of Fluids Engineering*, Vol. 99, March 1977, pp. 115–131.

[11] Whitfield, A., Wallace, F. J., and Atkey, R. C., "The Effect of Variable Geometry on the Operating Range and Surge Margin of a Centrifugal Compressor," American Society of Mechanical Engineers Paper 76-GT-98, 1976.

[12] Chima, R. V., and Yokota, J. W., "Numerical Analysis of Three-Dimensional Viscous Internal Flow," *AIAA Journal*, Vol. 28, No. 5, 1990, pp. 798–806.

[13] Hall, E. J., "Aerodynamic Modeling of Multistage Compressor Flow Fields—Part 1: Analysis of Rotor/Stator/Rotor Aerodynamic Interaction," American Society of Mechanical Engineers, Paper 97-GT-344, 1997.

[14]Dawes, W. N., "A Numerical Study of the 3D Flowfield in a Transonic Compressor Rotor with a Modeling of the Tip Clearance Flow," CP 401, AGARD, Neuilly sur Seine, France, pp. 21.1–21.12.

[15]Hah, C., and Wennerstrom, A. J., "Three-Dimensional Flowfields Inside a Transonic Compressor with Swept Blades," *Journal of Turbomachinery*, Vol. 113, No. 2, 1991, pp. 241–251.

[16]Adamczyk, J. J., Mulac, R. A., and Celestina, M. L., "A Model for Closing the Inviscid Form of the Average Passage Equations," American Society of Mechanical Engineers, Paper 90-GT-19, 1990.

[17]Escuret, J. F., and Garnier, V., "Numerical Simulations of Surge and Rotating Stall in Multi-Stage Axial-Flow Compressors," AIAA Paper 94-3202, June 1994.

[18]Rivera, C. J., "Numerical Simulation of Dynamic Stall Phenomena in Axial Flow Compressor Blade Rows," Ph.D. Dissertation, Dept. of Aerospace Engineering, Georgia Inst. of Technology, Atlanta, GA, 1998.

[19]Niazi, S., Stein, A., and Sankar, L. N., "Development and Application of a CFD Solver to the Simulation of Centrifugal Compressors," AIAA Paper 98-0934, Jan. 1998.

[20]Murray, R. M., "Active Control of Rotating Stall Using Pulsed Air Injection," MURI Workshop, Georgia Inst. of Technology, Atlanta, June 1998.

[21]Roe, P. L., "Approximate Riemann Solvers, Parameter Vectors and Difference Schemes," *Journal of Computational Physics*, Vol. 135, No. 2, 1997, p. 250.

[22]Beam, R., and Warming, R. F., "An Implicit Finite Difference Algorithm for Hyperbolic Systems in Conservation Law Form," *Journal of Computational Physics*, Vol. 22, Sept. 1976, pp. 87–110.

[23]Anderson, J. D., "Computational Fluid Dynamics," 1st ed., McGraw–Hill, New York, 1995, pp. 534–538.

[24]Spalart, P. R., and Allmaras, S. R., "A One-Equation Turbulence Model for Aerodynamic Flows," AIAA Paper 92-0439, Jan. 1992.

[25]Hathaway, M. D., Chriss, R. M., Wood, J. R., and Strazisar, A. J., "Laser Anemometer Measurements of the 3-D Rotor Flow Field in Centrifugal Compressor," NASA TP-3527, June 1995.

[26]Wood, J. R., Adams, P. W., and Buggele, A. E., "NASA Low Speed Centrifugal Compressor for Fundamental Research," NASA TM-83398, June 1983.

[27]Tweedt, D. L., Chima, R. V., and Turkel, E., "Preconditioning for Numerical Simulation of Low Mach Number Three-Dimensional Viscous Turbomachinery Flows," NASA TM ICOMP-97-11, Oct. 1997.

[28]Hathaway, M. D., and Wood, J. R., "Application of a Multi-Block CFD Code to Investigate the Impact of Geometry Modeling on Centrifugal Compressor Flow Field Predictions," *Transactions of the American Society of Mechanical Engineers*, Vol. 19, Oct. 1997, pp. 820–830.

[29]Hathaway, M. D., Criss, R. M., Wood, J. R., and Strazisar, A. J., "Experimental and Computational Investigation of the NASA Low-Speed Centrifugal Compressor Flow Field," *Journal of Turbomachinery*, Vol. 115, No. 3, 1993, pp. 527–542.

[30]Day, I. J., "Active Suppression of Rotating Stall and Surge in Axial Compressors," *Journal of Turbomachinery*, Vol. 115, No. 1, 1993, pp. 40–47.

[31]Weigl, H. J., Paduano, J. D., Frechette, L. G., Epstein, A. H., Greitzer, E. M., Bright, M. M., and Strazisar, A. J., "Active Stabilization of Rotating Stall and Surge in a Transonic Single Stage Axial Compressor," American Society of Mechanical Engineers, Paper 97-GT-411, 1997.

[32]Giffin, R. G., and Smith, L. H., "Experimental Evaluation of Outer Case Blowing or Bleeding of Single Stage Axial Flow Compressor, Part I—Design of Rotor and Bleeding and Blowing Configurations," NASA CR-NAS 3-7618, April 1966.